Influence of Molecular Weight on Molecular Ordering and Proton Transport in Organized Sulfonated Polyimide Thin Films

Karthik Krishnan,[†] Hiroko Iwatsuki,[‡] Mitsuo Hara,[‡] Shusaku Nagano,[§] and Yuki Nagao[†,*]

[†] School of Materials Science, Japan Advanced Institute of Science and Technology, 1-1 Asahidai, Nomi, Ishikawa 923-1292, Japan.

[‡] Department of Molecular Design & Engineering Graduate School of Engineering, Nagoya University, Furo-cho, Chikusa, Nagoya 464-8603, Japan

[§]Nagoya University Venture Business Laboratory, Nagoya University, Furo-cho, Chikusa, Nagoya 464-8603, Japan

Abstract

The effect of molecular ordering and ordered domain size on molecular weight dependent proton conductivity in well-organized sulfonated polyimide (SPI) thin films has been investigated using both low molecular weight (LM_w, M_w= 1.3 × 10^4) and high molecular weight samples (HM_w, M_w= 2.6 × 10^5). Analyses of the films by grazing incidence small angle X-ray scattering (GISAXS) revealed that the HM_w SPI film exhibits the higher degree of inherent liquid crystalline-like lamellar ordering, and that it is consistent with a preferential in-plane main chain packing. Such molecular ordering and the in-plane oriented structure can have considerable influence on the proton transport characteristics in thin films. The larger ordered domains in the HM_w SPI thin film with a thickness of approximately 500 nm shows the significant proton conductivity enhancement to a value of 2.6 × 10^{-1} S/cm (at 25 ºC and 95% relative humidity), which is more than an order of magnitude higher value than that of the smaller ordered domains in the LM_w SPI thin film with less molecular ordering. The larger ordered domains in the HM_w SPI thin film influence the conducting characteristics attributable to the fewer liquid crystalline-like domain boundaries relative to LM_w SPI films because the smaller ordered domains in the

LM_w SPI thin film more obviously exhibit large-scaled domain boundaries, which can disrupt the fast ion transportation.

Keywords: lyotropic liquid property, molecular ordering, organized structure, confined property, molecular weight

1. Introduction

Sulfonated polyimides (SPI) containing alkylene segments both in main and side chains are found to be the essential polymer electrolytes in fuel cells owing to the substantial stability and high proton conductivity.[1,2] The typical polymer electrolyte for fuel cell is well known to require the high proton conductivity, mechanical and chemical integrity, low permeation to gases and limited swelling.[3–5] The hydrophilic sulfonic acid group contained in SPI usually forms ionic channels upon sorption of water, which promotes the proton transport.[6,7] In general, the degree of sulfonation and interaction strength of water molecules facilitates proton transport characteristics in polymer electrolytes during fuel cell operation. However, excessive swelling may arise when the interaction is stronger between water molecules and sulfonic acid group, which significantly reduces the stability and continuous proton transport paths.[8,9] Therefore, confinement of the polymer structure for enhancing property characteristics constitutes an important issue in the development of solid H_2/O_2 fuel cells.[10–14] In fuel cell infrastructure, the development of polymer electrolytes for higher proton transportation along with substantial stability has been done mostly through chemical modification.[15–18] Instead of chemical modification, a rational design of polymer electrolytes requires fundamental understanding of the role of confined polymer structure in influencing proton transport characteristics. Recent investigations have been

conducted to elucidate the well-organized polymer structure and their interfacial confinement for enhancing the proton transport and stability characteristics.[19] How the chain alignment and long-range periodicity of polymer chains control the transport property and how stability leads to the development of solid polymer electrolytes are two important questions that must be answered. To date, various reports describe studies of the macroscopic structural ordering to enhance the proton transport, but they are insufficient to explain the interfacial charge transport characteristics in confined thin film polymer structures.[20-23]

In conjugated polymer films, the anisotropic charge transport occurs most efficiently either in the direction of chain stacking, or along the polymer backbone, which is the fastest transportation direction inside an aggregate. During film confinement, a higher degree of polymer packing and domain ordering is also favorable for higher charge transport. Most commonly, the strong polymer chain interactions promote the favorable polymer packing that often results in large-scaled domain order.[24,25] Interchain interaction and domain ordering likely are governed by many parameters such as processing conditions, solubility limit, surface state, and molecular weights.[26-28] Amongst the molecular weight and solubility parameters emerged to control the polymer packing, where polymers of higher solubility promote face-on packing and less-soluble polymers favors edge-on packing.[26] To estimate the SPI polymer packing on proton transport property, we specifically examine the molecular weight that controls the ordered domains during SPI film formation. Generally, aromatic polyimide (API) possesses a rigid planar molecular structure that exhibits higher in-plane orientation than the non-planar molecular structures.[29] The interchain packing and π-stacking of imide and phenyl groups in APIs vary considerably according to differences in aggregation structures, e.g., crystalline, liquid-crystalline (LC) like and amorphous. In addition, the absence of large-scale three-dimensional ordered domains in the

API films suggesting mesomorphic ordering between the amorphous and crystalline phases can be interpreted as reflecting the existence of lyotropic LC like ordered domains.[29]

The main objective of this report is to ascertain the relation between lyotropic LC domain ordering and proton conductivity on SPI thin films. The discussion also provides new insights relates to the correlation between the lyotropic LC domain structure and molecular weight of SPI thin films. The larger ordered domains in a high molecular weight (HM_w) SPI thin film exhibits higher proton conductivity than the smaller ordered domains in low molecular weight (LM_w) SPI thin film. The increase in LC domain structure in the highly oriented HM_w SPI thin film strongly contributes the proton conductivity enhancement.

2. Experimental

2.1. Materials

3,3'-Dihydroxybenzidine, propanesultone, and pyromellitic dianhydride (PMDA) were used as received from Tokyo Chemical Industry Co. Ltd., Japan. Acetic anhydride, acetic acid, methanol, and acetone were purchased from Wako Pure Chemical Inds. Ltd., Japan. Hydrochloric acid (Nacalai Tesque Inc., Japan), sodium hydroxide (Kishida Chemical Co. Ltd., Japan), m-cresol, and triethylamine (TEA, Kanto Chemicals Co. Inc., Japan) were used as received.

2.2. Synthesis of SPI

SPIs with various molecular weights were prepared using the same polymerization scheme (Scheme 1). The reaction was initiated by acetylation process using 3,3'-dihydroxybenzidine as the starting material because the amino groups in 3,3'-dihydroxybenzidine were protected by acetylation. In a typical reaction, 5 g 3,3'-dihydroxybenzidine was mixed with 1.5 ml acetic acid, 79 ml acetic anhydride, and 200 ml distilled water. This mixture was stirred at 70 °C for 1 hr.

After the mixture cooled to room temperature, the precipitate was collected and separated using centrifugation. The products were washed several times with acetone to remove unreacted species, and the obtained precipitate was dried under vacuum. NMR study was used to confirm the incorporation of the acetyl functional group. Prior to each step, all prepared monomers were characterized by ^{1}H NMR.

Acetylated 3,3'-dihydroxybenzidine (6 g) was sulfonated using 7.3 g propanesultone as the reagent. Consequently, 2.4 g sodium hydroxide was dissolved in methanol (150 ml), and then it was poured into the propanesultone and the acetylated 3,3'-dihydroxybenzidine containing mixture. The overall reaction mixture was refluxed at 80 °C under an argon atmosphere for 6 hr. A pale-white precipitate was received and washed several times with cold methanol. For ion exchange process, the obtained monomer was dissolved completely in distilled water. An ion exchange step was performed using Amberlyst. Using a rotary vacuum evaporator, the ion-exchanged monomers were separated and dried under vacuum. To remove the acetate groups, we added concentrated hydrochloric acid (HCl) to the final product obtained from the step described previously. Then we refluxed the mixture at 120 °C for 1 hr under an inert atmosphere. After the mixture was refluxed, the cooled product was heated at 150 °C to evaporate the concentrated HCl. The HCl vapor was neutralized carefully with a concentrated base.

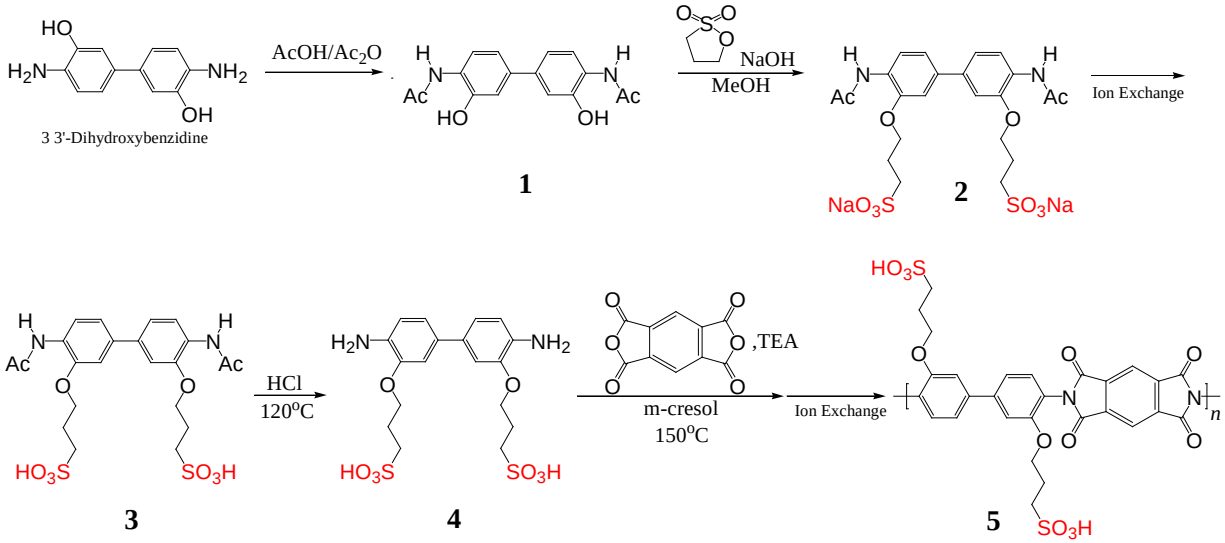

Scheme 1. Steps used for synthesizing sulfonated polyimide

Polymerization was conducted using the prepared sulfonated monomers (0.43 g), PMDA (0.22 g), m-cresol (5 ml), and TEA (0.3 ml). m-Cresol was used as the solvent. The polymerization reaction was processed under an argon atmosphere at a constant temperature of 150 °C for 5 hr. The polymerized product was collected after washing with cooled acetone. The final product was subjected again to an ion-exchange process using Amberlyst. In our preparation, we obtained the SPI polymers with various molecular weights. Among them, we selected the LM_w (1.3×10^4) and HM_w (2.6×10^5) SPI samples for comparative study. Both polydispersity indexes are 11-12 for Mw/Mn. The degree of sulfonation for the final product was estimated from ^{1}H NMR data: it was more than 98%. The calculated ion exchange capacity (IEC) was 3.1 mequiv/g.

2.3. Gel permeation chromatography (GPC)

Gel permeation chromatography (GPC, LC-2000plus; Jasco Inc.) was used. Response to the HPLC system control of up to four through the (controller) LC-Net II / ADC enables simultaneous recording of four chromatograms per system. A DMF-, H_2O-, CH_3COOH- and $NaNO_3$-containing mixture was used as the eluent at a flow rate of 1.0 mL min^{-1}. The polymer

solutions were filtered through a 0.50 μm PTFE hydrophobic filter before being injected into the column. The molecular weight was calibrated with a polystyrene standard.

2.4. Preparation of thin films

Active ACT−200 spin-coater was used to prepare nanostructured SPI thin films cast on quartz substrates. The substrates were subjected to several cleaning processes prior to film deposition. Plasma treatment was performed using a vacuum plasma system (Cute-MP; Femto Science Inc., Korea) to improve surface hydrophilicity. Thicknesses of the thin films were measured using a surface profiler (P-15 profiler; KLA-Tencor Corp.).

2.5. Polarized optical microscopy (POM)

POM was conducted with crossed polarizers to observe the liquid crystalline-like ordered domains and to ascertain their size in the polymer films (BX51-P; Olympus Corp. / DP28 camera; Olympus Corp.) Data were recorded with Cellscan controller software.

2.6. Grazing incidence small angle X-ray scattering (GISAXS)

GISAXS measurements were performed using an X-ray diffractometer (FR-E; Rigaku Corp.) with an R-AXIS IV two-dimensional (2D) detector. The sample stage was composed of the goniometer and a vertical stage (ATS-C316-EM/ALV-300-HM; Chuo Precision Industrial Co. Ltd.) with a humidity-controlled cell. The typical cell holds polyimide film (Kapton) windows and the humidity-controlled cell. Nitrogen carrier gas was used as received, without further dehumidification, from the gas cylinder to control the humidity. We used Cu Kα radiation (λ = 0.1542 nm) with a beam size of approximately 300 μm × 300 μm. The camera length was 300 mm. The incidence angle was chosen in the range from 0.20° to 0.22°. Diffraction patterns of the out-of-plane and in-plane directions obtained from thin film samples were used to extract information related to the presence of liquid crystalline lamellar structures and the repeating unit

of the polyimide main chain. For 1-D out-of-plane and in-plane patterns, the integrated regions were taken between -0.5° – 0.5° as 2θ from the center (0°) and the width of 1° as 2θ, respectively.

Small-angle X-ray scattering (SAXS) measurements in the bulk state were performed using the same X-ray diffractometer. A dry sample was placed in a capillary tube and was irradiated with the X-ray beam without further adjustments.

2.7. p-Polarized multiple angle incidence resolution spectrometry (p-MAIRS)

p-MAIRS technique has been used to investigate the polymer orientations of the nanostructured SPI thin films on Si wafers in both the in-plane and out-of-plane directions.[30,31] The surface of the original Si wafer was oxidized before measurements. Then p-MAIRS measurements were collected with a Fourier-transform infrared (FTIR) spectrometer (Nicolet 6700; Thermo Fisher Scientific Inc.) equipped with a mercury cadmium telluride (MCT) detector. Single-beam spectra were collected from 38° to 8° in 6° steps between the angle of incidence. Thicknesses of the films prepared on the oxidized Si substrate used for this measurement were approximately 500 nm.

2.8. Conductivity measurements of thin films

The proton conductivity of SPI thin films were examined through impedance spectroscopy measurements using a frequency response analyzer (SI1260; Solartron Analytical) equipped with a high-frequency dielectric interface (SI1296; Solartron Analytical). The relative humidity (RH) and temperature were controlled using a computer-controlled environmental test chamber (SH-221; Espec Corp.). For thin film conductivity measurements, two-probe method was used to obtain proton conductivity on the surface parallel to the film. Gold contacts were used as the thin film electrodes for the conductivity measurements. Impedance data were collected for

frequencies of 1 Hz and 10 MHz, with an applied alternating potential of 50 mV. Thin-film conductivity (σ) was calculated as,

$$\sigma = \frac{d}{Rlt} \tag{1}$$

where *d* signifies the distance between the gold electrodes, *R* is the resistance value obtained directly from the impedance measurement, *l* denotes the contact electrode length, and *t* represents the thickness of the film.

2.9. X-ray reflectivity

The X-ray reflectivity measurements were carried out by a high-resolution X-ray diffractometer (ATX-G; Rigaku Corp.) with X-ray wavelength λ= 0.1542 nm (Cu Kα) generated from a Cu rotating anode (50 kV, 300 mA). X-rays were collimated by a parabolic multilayer mirror and slit collimators.

3. Results and discussion

3.1. LC ordered domain and size

In the previous study, the oriented organized structure has been suggested by the GISAXS and IR measurements. To elucidate whether the lyotropic LC domain morphologies on SPI thin films are observed or not, polarized optical microscopy was used. Figure 1 shows the polarized optical microscope images for both LM_w and HM_w SPI thin films. The LC morphology on the thin films was identified under cross polarized light when the sample was rotated from 0º (Figure 1a and 1c) to 45º (Figure 1b and 1d) with respect to the direction of polarized light. These images show that the HM_w SPI thin film engenders the increase in domain size and macroscopic alignment over a large area, which suggests that the LC region within the domains is well oriented. Smooth proton transport occurs with low activation energy in the highly conductive domain, but harder

transport might occur in between the inter-domain with higher activation energy. This domain size difference between the LM_w and HM_w SPI thin films could be related with the internal structural difference. Therefore *in situ* GISAXS analysis was carried out.

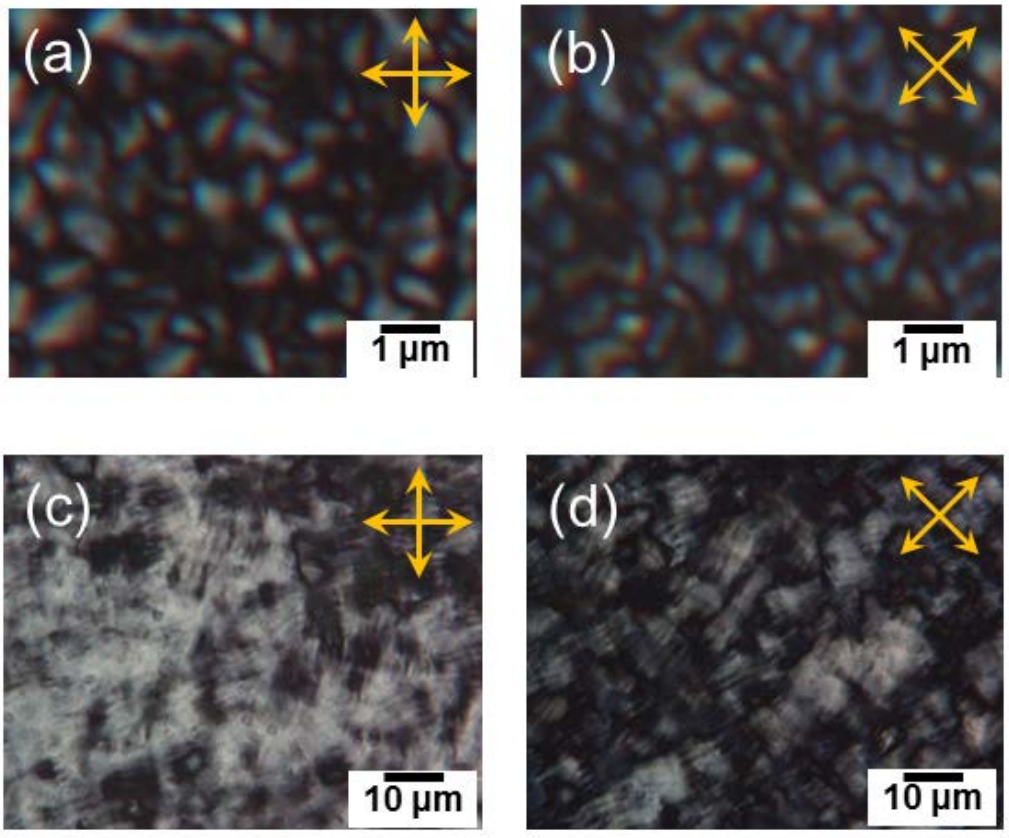

Figure 1. Polarized optical micrograph images of both (a and b) LM_w and (c and d) HM_w SPI thin films at 0º and 45º, respectively.

3.2. Structural interpretation using *in situ* GISAXS

Differences in the molecular packing and crystalline order obtained by varying the molecular weight in SPI thin films were investigated using *in situ* GISAXS analysis with humidity control. The 2D scattering images in the RH-dependent *in situ* GISAXS measurements were shown, respectively, in Figures S4a–S4d and Figures 2a–2d for HM_w and LM_w SPI thin films. Figures S4e, S4f and Figures 2e, 2f respectively show a series of 1D scattering profiles for HM_w and LM_w SPI thin films with various RH measured both in in-plane and out-of-plane directions. The

scattering arcs at the positions of 0.75 and 0.84 $Å^{-1}$ were artifacts caused by diffraction of the Kapton film used as the windows for the humidity-controlled GISAXS cell.

In the wide angle regions, the 2D GISAXS patterns of both LMw and HM_w SPI thin films at 0% RH condition (dry condition) exhibit strong semicircle scattering at q_z = 1.4 $Å^{-1}$ of d = 0.4 nm (Figures 2a, 2f, S4a and S4f [19]). The scattering intensity of the semicircles is anisotropic unlike the isotropic amorphous halo scattering observed by measuring only a quartz substrate (Figure S5 and S6). The strong intensity of the broad intense peak is observed toward the out-of-plane azimuthal direction, indicating that the repeating ordered structure is formed perpendicularly to the substrate plane in the SPI film. Ando *et al*. reported the different types of ordered polyimide structures in thin films using detailed GISAXS analysis.[32] Backbones and conjugated planes of aromatic polyimides in thin films in ordered domains parallel to the substrate plane, where the scatterings corresponding to the main chain packing (ch-pack) and conjugated plane stacking (π stack) were observed in the out-of-plane direction with d-spacing ranging from 0.36 to 0.57 nm.[32] The broad out-of-plane peak can be assigned to the interchain packing in the thin film. In the small angle region, the in-plane peak profiles of both LM_w and HM_w exhibit sharp scattering peak at q_y = 0.37 $Å^{-1}$ of d = 1.7 nm at 0% RH condition (Figure 2e and S4e). The in-plane scattering is attributed to the periodic monomer unit length for the polyimide chain units for the appropriate positions of the corresponding polyimides.[32]

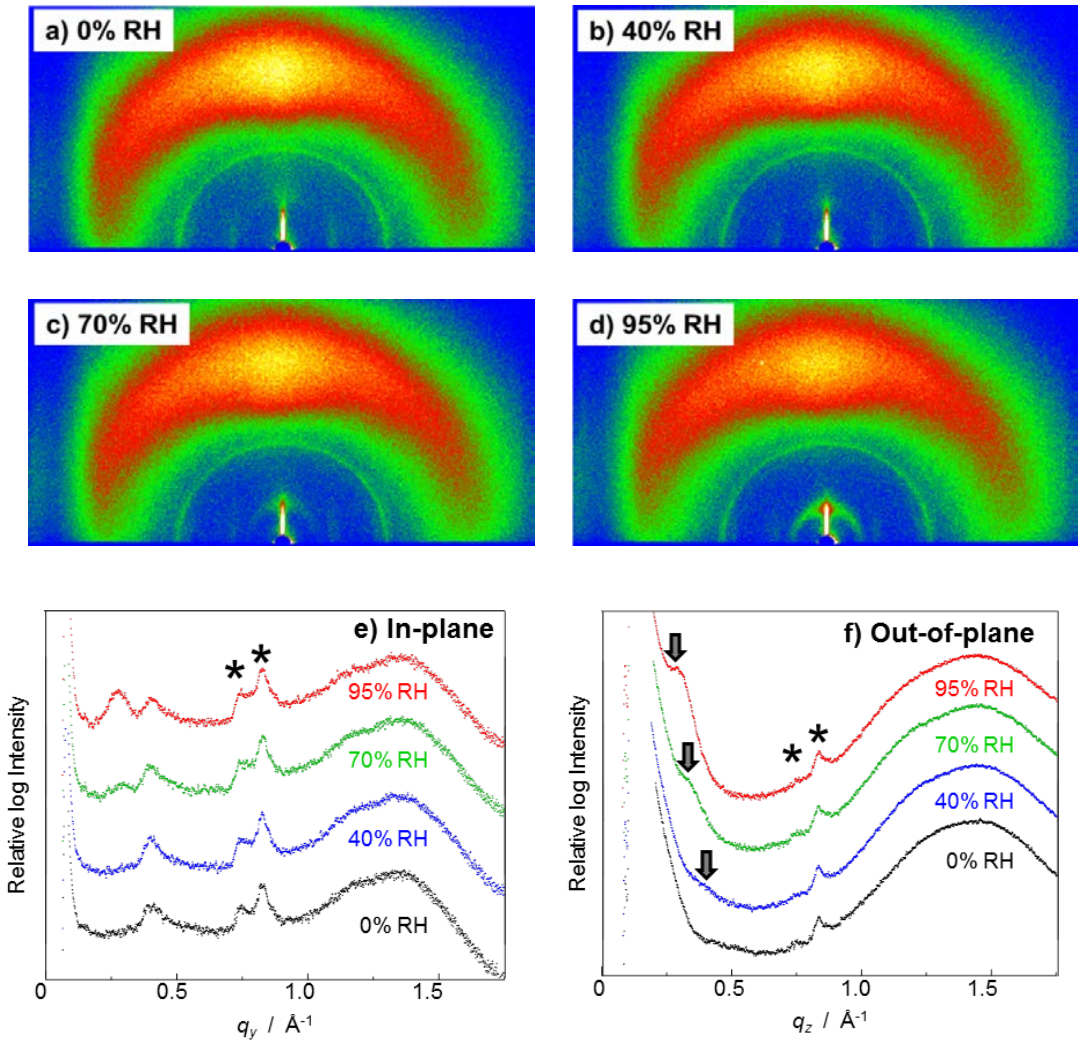

Figure 2(a, b, c and d). The 2D GISAXS patterns at 0% RH, 40% RH, 70% RH and 95% RH, respectively, and the humidity-dependent 1D GISAXS profiles in the (e) in-plane and (f) out-of-plane directions of the LM_w SPI thin film. The peak indicated by arrows in Fig. 2f is discussed in the manuscript. The mark of * is Kapton window.

The present out-of-plane and in-plane scatterings can be assigned respectively to the interchain packing and the periodic monomer unit length for the SPI main chains.[19] Furthermore, in dry condition, the HM_w SPI thin film exhibits another small angle scattering at 0.39 Å^{-1} (d = 1.6 nm) is observed in out-of-plane direction. Our earlier work has shown that the out-of-plane scattering peak is attributable to the lamellar structure in the in-plane stacked hydrophobic polyimide

backbone with the out-of-plane bridging of hydrophilic sulfonated side chains as shown in Figure 3a.[19] The previous birefringence observation of the polarized optical microscope is explainable by this internal oriented structure. At high RH conditions, the small angle out-of-plane peak enhanced and shifted to the smaller angle region (Figure S4f). At 95% RH, the out-of-plane peak reached 0.34 $Å^{-1}$ (d = 1.8 nm); it was markedly enhanced relative to the X-ray specular peak. The in-plane peak profile is almost unchanged by humidity. These results indicate that the inter-lamellar hydrophilic sulfonated layer during the high humidity region is hydrated selectively, thereby enhancing of molecular ordering and the expansion of lamellar spacing to the out-of-plane direction as shown in Figure 3b.[19]

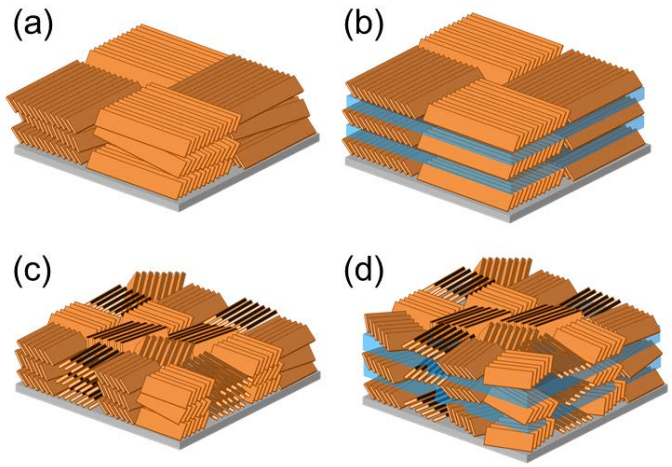

Figure 3. Schematic views of the degree of the molecular ordering and ordered domain size. (a) HM_w SPI thin film in dry condition with relatively larger domain size. (b) HM_w SPI thin film in high humidified condition with improved molecular ordering in the out-of-plane direction. (c) LM_w SPI thin film in dry condition with less ordering structure and relatively smaller domain size. This is an expected structure because of absence of out-of-plane scattering at 0.39 $Å^{-1}$ (d = 1.6 nm). (d) LM_w SPI thin film in high humidified condition with improved molecular ordering in the out-of-plane direction and relatively smaller domain size.

For the LM_w SPI thin film under a dry condition (Figures 2a, 2e, 2f), we were able to obtain fundamentally identical 2D scattering image to that of the HM_w SPI thin film, except in the absence of out-of-plane scattering at 0.39 $Å^{-1}$ (d = 1.6 nm). In the humidified condition, however, new scatterings are recognized around the small angle region in the out-of-plane peak profile with overlapping of direct X-ray specular peak. The arc scatterings are observed in the out-of-plane small angle region from 2D profiles of Figure 2c and 2d. As humidity increases, the arc scattering enhanced and shifted to smaller angle. This change by the humidity can be attributed to the amphiphilic lamellar expansion.

To clarify the difference of the scattering aspects between the LM_w and HM_w SPI thin films, Figure 4 summarize 1D GISAXS profiles of the LM_w and HM_w SPI thin films in the out-of-plane (a) and in-plane (b) directions under dry and humid conditions. The absence of the small angle scattering due to the inter-lamellar structure in the LM_w SPI thin film indicates that the lower molecular weight leads to higher thermal fluctuation of LC structure by thermodynamic driving force. As evidence, one additional scattering peak is apparent in in-plane pattern around 0.34 $Å^{-1}$ (d = 1.8 nm) in the LM_w SPI thin film of the 95% RH condition (Figure 4a). This peak corresponds to the same scattering peak around 0.34 $Å^{-1}$ (d = 1.8 nm) in the out-of-plane pattern (Figure 4b) and is attributable to the nature of lamellar structure. The peak intensity corresponding to the amphiphilic lamellar structure is weak, even in highly humidified conditions (95% RH) in the LMw SPI thin film. This result suggests the LM_w SPI thin film has a less structural ordering comparing with the HM_w SPI thin film. The smaller domain size shown by polarized optical microscope is explainable by this less-structured ordering in the LM_w SPI thin film as shown in Figures 3c and 3d.

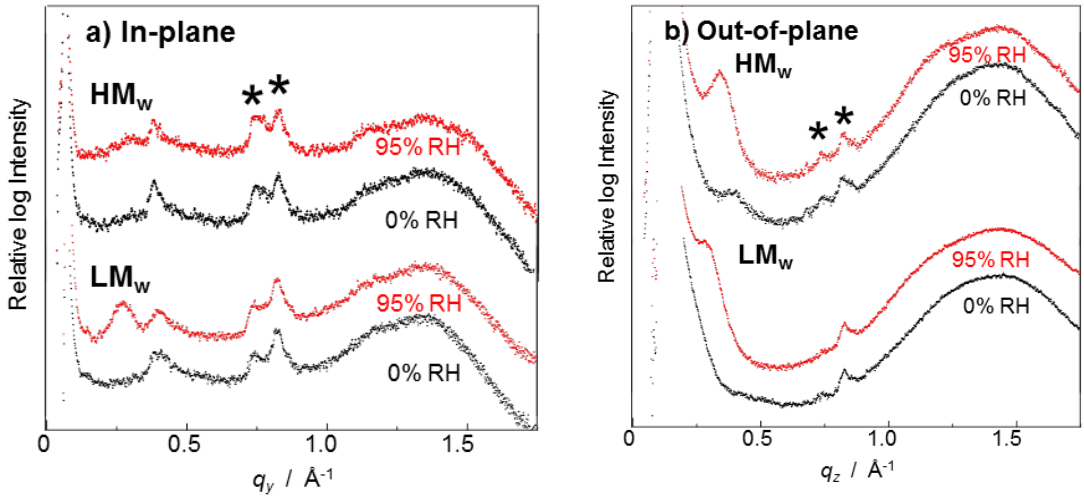

Figure 4. The humidity-dependent 1D GISAXS profiles in the (a) out-of-plane and (b) in-plane directions of the SPI thin films. The marks of * indicate the scattering from the Kapton windows.

The intensity enhancement (half order magnitude) and scattering peak shift (from 0.42 to 0.34 $Å^{-1}$) with humidity involve the lamellar expansion (Figure S7a and S7b) and ordering of the amphiphilic lamellar structure to the out-of-plane direction similar to a lyotropic liquid crystalline phase. Because of the strong interaction between the sulfonic acid side chain units and water as well as the hydrophobic packing of the SPI main chains, the formation of the lyotropic lamellar structure is explainable for water uptake. This structural change is completely reversible versus relative humidity. This SPI film exhibits a humidity dependent self-assembly structure. Higher in-plane proton conductivity along the polymer chains can be attained from in-plane ordering and expansion of the amphiphilic lamellar structure under high-humidity conditions.

3.3. Polymer orientation using p-MAIRS

The p-MAIRS technique coupled with IR spectroscopy used in this investigation offers a significant molecular information resolved by the in-plane and out-of-plane spectra, depending on the molecular orientation.[30,31] Figure 5 shows p-MAIR spectra of LM_w and HM_w SPI thin

films, measured in both in-plane and out-of-plane modes. The observed vibrational modes at 1381 and 1504 cm^{-1} are attributed to the C−N bonds of the imide groups and to phenyl C−C stretching vibration, respectively. Two vibrational modes at approximately 1726 and 1781 cm^{-1} correspond to the C=O asymmetric and symmetric stretching vibrations of imide groups, respectively.[19,33,34] No peak corresponds to the presence of polyamic acid, which is normally located at 1530 and 1690 cm^{-1}. The peak of polyamic acid at 1530 cm^{-1} is ascribable to the stretching of C−N bonds of amide. The peak at 1690 cm^{-1} results from the carboxylic acid or amide group of C=O bonds.

According to the band positions and relative intensity between in-plane and out-of-plane vibrational modes of p-MAIR spectra, the molecular orientation can be ascertained.[35–37] In general, the strongest absorbance occurs when the electric field vector of the IR rays and the orientation of the molecular vibration become parallel. However, the randomly oriented polymer structure in thin films would exhibit identical in-plane and out-of-plane vibrational modes. Occurrence of greatly deviated in-plane and out-of-plane vibrational modes of SPI obviously differentiate the anisotropic molecular orientation in thin films. The absorbance strength of the in-plane component is higher than the out-of-plane component, indicating that the highly oriented polymer chains are parallel to the substrate surface. Spectra of HM_w and LM_w SPI thin films show very similar shapes. The main chains of both HM_w SPI and LM_w SPI thin films are oriented parallel to the surface. Usually, the higher frequency carbonyl group (C=O) vibrations are the most expedient for use in characterizing the orientation distribution. Because of the high in-plane orientation of polymer chains, the C=O asymmetric stretching possesses higher intensity than the phenyl stretching.[38] To check the difference of the orientation of the C=O asymmetric

stretching between the HM_w SPI and LM_w SPI thin films, the degree of the orientation was estimated according to the following equation,[31]

$$\varphi = \tan^{-1}\sqrt{\frac{2I_{IP}}{I_{OP}}} \quad (2)$$

Where I_{IP} and I_{OP} are the in-plane and out-of-plane band intensity of C=O group and φ is the orientation angle from the surface normal. The distribution of the orientation cannot be analyzed from this analysis. The obtained ~~orientation~~ angles of the C=O asymmetric stretching are 44° and 40°, respectively, in the HM_w SPI and LM_w SPI thin films. These values are not so different. Other orientation angles of the C−C and C−N groups are also same values. So the large difference of the molecular orientation between the HM_w SPI and LM_w SPI thin films has not been obtained.

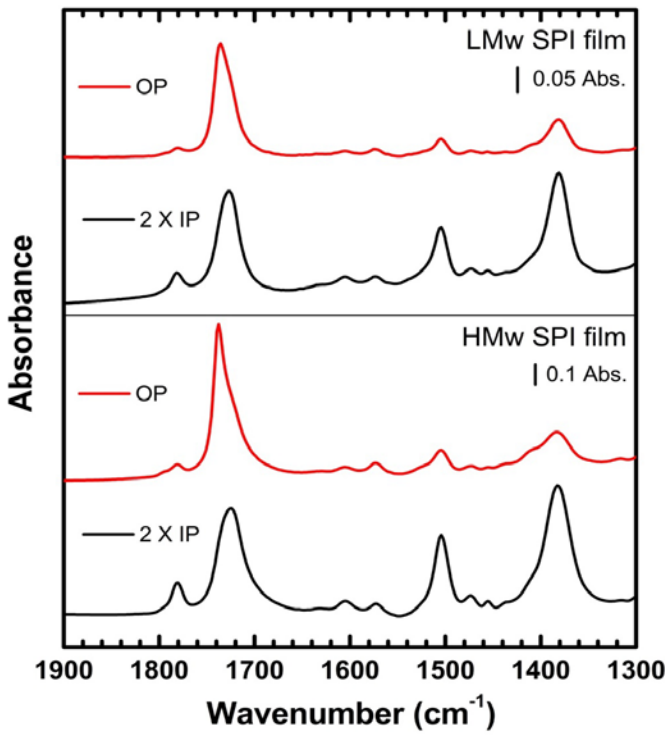

Figure 5. In-plane (IP) and out-of-plane (OP) profiles of p-MAIR spectra for both LM_w and HM_w SPI thin films. Reasons for the double IP absorbance are explained in the literature.[14,31]

3.4. Structure-dependent proton transport property

Figure 6 depicts proton conductivity plots for SPI thin films as a function of molecular weight. The proton conductivity for HM_w SPI thin film showed a remarkably higher value of 2.6×10^{-1} S/cm (at 25 ºC and 95% RH).[19] A linear increase in conductivity is observed by the increase in RH, which is similar for both LM_w and HM_w SPI thin films. However, the proton conductivity of HM_w SPI thin film manifests more than an order of magnitude higher value than that of the LM_w SPI thin film (1.0×10^{-2} S/cm at 25 ºC and 95% RH). From the proposed lamellar structure, the side chain sulfonic acid functional groups aggregate to form continuous hydrophilic domains parallel to the surface at the high humidity region that selectively hydrated upon the adsorption of water molecules. Such continuously formed hydrophilic domains in the highly ordered system promote the marked enhancement of conductivity. It is also expected that variation of structural ordering, or the change in the degree of liquid crystalline-like polymer packing by changing the polymer molecular weights, causes a huge difference in proton conductivity between these two SPI thin films. Elucidation of this structural effect by varying the polymer molecular weight is crucially important to correlate the structure-property relation by which one can readily tune the polymer property characteristics without the need for general chemical modifications.

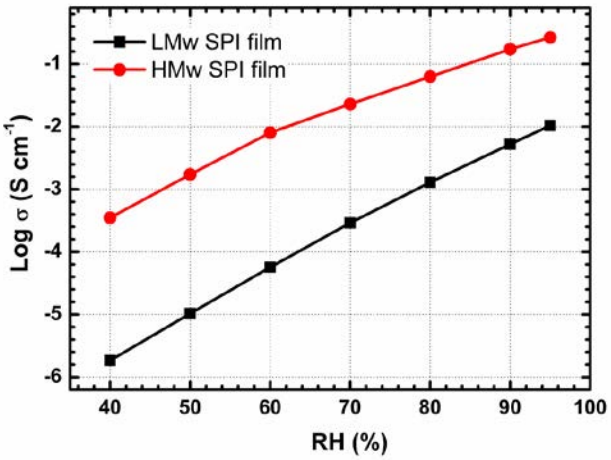

Figure 6. RH-dependent proton conductivity plots for both LM_w and HM_w SPI thin films.

Figure 7 shows temperature-dependent proton conductivity plots for both LM_w and HM_w SPI thin films. The conductivity data were measured using various temperatures and constant RH value of 90%. Substantial deviation in the conductivity is obtained between the LM_w and HM_w SPI thin films. Varying the temperature from 20 ºC to 80 ºC elevates the conductivity from 4.8 × 10^{-3} to 1.8 × 10^{-2} S/cm for LM_w SPI thin film, and from 1.4 × 10^{-1} to 2.8 × 10^{-1} S/cm for HM_w SPI thin film. Differences in the conductivity between LM_w and HM_w SPI thin films are explainable by the activation energy (E_a) of proton hopping. According to the Arrhenius equation (3) for the ionic conduction, the estimated E_a for both the LM_w and HM_w SPI thin films are 0.20 eV and 0.10 eV, respectively.

$$\sigma T = \sigma_0 \, exp\left(\frac{-E_a}{RT}\right) \tag{3}$$

Therein, E_a, R, T, and σ_0 respectively represent the activation energy, gas constant, temperature and pre-exponential factor. This difference in proton conductivity cannot be explained only by the chemical formula as a primary structure. The higher-order architectures with the polymer packing and liquid crystalline-like ordering in SPI thin films can strongly engender proton transport characteristics.

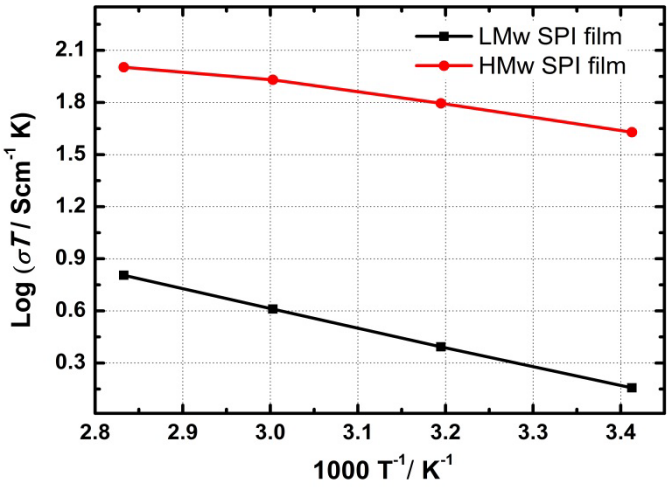

Figure 7. Temperature-dependent proton conductivity plots for LM_w and HM_w SPI thin films.

The ordering and orientation of the liquid crystalline-like nanostructure play important roles in improving the proton conductivity. In the present case, the highly ordered HM_w SPI thin film exhibits one order of magnitude higher proton conductivity than that of the less-ordered LM_w thin film, mainly because of the difference of degree of ordered domain size by the change in molecular weight.

3.5. Confirmation of molecular weight contribution to the proton transport property

Further investigations were conducted to elucidate why the proton conductivity differs greatly between LM_w and HM_w SPI thin films. Structural differences in powder samples as bulk materials were examined using SAXS study under dried conditions (Figure S8, Supporting Information). It is necessary to ascertain and to correlate how molecular ordering in the bulk case affects the scattering profile. It is particularly interesting that both samples show similar 2D SAXS and 1D SAXS patterns. The scattering peak in the lower angle region at approximately 0.40 $Å^{-1}$ (q) corresponds to the repeating units of the main chain polymer and the dried lamellar phase. The corresponding d-spacing value for this peak is 1.5 nm. Both are similar structure between HM_w bulk SPI and LM_w bulk SPI. Therefore the original structure from the bulk sample is found to be very similar.

It is important that the ordered domain size from POM observations varied considerably with molecular weight when the SPI is confined into a thin film. Therefore, we strove to ascertain how the proton concentration and density could change while the SPI was confined into thin film. X-ray reflectivity study was conducted to estimate the proton concentration by variation of the density as function of molecular weight as shown in Figure S9. Table 1 presents data analyzed from X-ray reflectivity, which are quite similar density values between the LM_w and HM_w SPI

thin films. Because of their same chemical structure, the densities of both LM_w and HM_w SPI thin films are almost equal. The *in situ* IR analysis was also conducted as shown in Figure S10. Both SPI thin films show almost identical absorbance, which suggests that numbers of adsorbed water molecules of HMw and LM_w SPI thin films are not so different from each other. Therefore, the proton concentrations might also be similar or equal.

Table 1. Density of both the LM_w and HM_w SPI thin films by X-ray reflectivity.

	ρ (g/cm^3)
LM_w SPI thin film	1.54
HM_w SPI thin film	1.57

Therefore, we propose that the lyotropic lamellar structure of the larger liquid crystalline-like packing in the HM_w SPI thin film can provide long-range proton conducting in-plane channels, which is more beneficial for obtaining the enhanced proton transport in highly ordered systems. In the LM_w SPI film at 95% RH, the scattering peak corresponding to the sudden change of lyotropic lamellar structure in in-plane direction (Figure 3b), suggesting that the randomly oriented proton channels arose from the unstable less-ordered domains.

In summary, an organized structure with high proton conduction was achieved using the lyotropic LC property. This macroscopic proton transport is strongly dependent on the degree of the molecular ordering and LC domain size in highly oriented SPI thin films. We demonstrated how organization of the structure as a higher-order structure can contribute to the proton transport property. This finding provides a new strategy for the development of the highly

proton-conductive materials from the viewpoints of the protonic devices in future. This proton-conductive organized structure can open the door to structure-driven protonics.

4. Conclusion

Influence of molecular weight on molecular ordering and proton transport in well-organized SPI thin films has been demonstrated. Results of this study indicate that the ordering and orientation of the LC domains in a thin film nanostructure with different molecular weights play important roles for enhancing proton conductivity. The most obvious explanation for the observed gain in proton conductivity derives from improvement of the degree of the molecular ordering and LC domain size. Both HM_w and LM_w SPI thin films exhibit the highly oriented polymer chains in the in-plane direction and organized lyotropic lamellar structure. However, the smaller LC domains with the less molecular ordering of the LM_w SPI thin films reduce the proton transport. On the basis of diffraction profiles and POM observations, the degree of lyotropic LC like ordering and domain size increases in the HM_w SPI thin film.

Acknowledgments

This work was supported in part by the Nanotechnology Platform Program (Molecule and Material Synthesis) of the Ministry of Education, Culture, Sports, Science and Technology (MEXT), Japan. This work was financially supported by the Japan Society for the Promotion of Science (JSPS) through the Funding Program (GR060) for Next Generation World-Leading Researchers (NEXT Program), initiated by the Council for Science and Technology Policy (CSTP). This work was partially supported by the research funds of The Kyoto Technoscience Center and the Research Foundation for the Electrotechnology of Chubu (REFEC).

Supporting information

Synthesis and characterization of sulfonated polyimide, GISAXS data, bulk SAXS data, X-ray reflectivity (XRR) data, relative humidity dependent FTIR-ATR, AFM, and GISAXS data for the quartz substrate. This material is available free of charge via the internet at http://pubs.acs.org.

Author information

Corresponding author

*ynagao@jaist.ac.jp Phone: +81(Japan)-761-51-1541, Fax: +81(Japan)-761-51-1149, Address: 1-1 Asahidai, Nomi, Ishikawa 923-1292, Japan

Notes

The authors declare no competing financial interest.

References

(1) Asano, N.; Aoki, M.; Suzuki, S.; Miyatake, K.; Uchida, H.; Watanabe, M. Aliphatic/aromatic Polyimide Ionomers as a Proton Conductive Membrane for Fuel Cell Applications. *J. Am. Chem. Soc.* **2006**, *128*, 1762–1769.

(2) Saito, J.; Miyatake, K.; Watanabe, M. Synthesis and Properties of Polyimide Ionomers Containing 1H-1,2,4-triazole Groups. *Macromolecules* **2008**, *41*, 2415–2420.

(3) Yang, J. S.; Cleemann, L. N.; Steenberg, T.; Terkelsen, C.; Li, Q. F.; Jensen, J. O.; Hjuler, H. A.; Bjerrum, N. J.; He, R. H. High Molecular Weight Polybenzimidazole Membranes for High Temperature PEMFC. *Fuel Cells* **2014**, *14*, 7–15.

(4) Jang, S. Y.; Han, S. H. Characterization of Sulfonated Polystyrene-block-poly(ethyl-ran-propylene)-block-polystyrene Copolymer for Proton Exchange Membranes (PEMs). *J. Membr. Sci.* **2013**, *444*, 1–8.

(5) Yan, X.; Gu, S.; He, G.; Wu, X.; Benziger, J. Imidazolium-functionalized Poly(ether ether ketone) as Membrane and Electrode Ionomer for Low-temperature Alkaline Membrane Direct Methanol Fuel Cell. *J. Power. Sources* **2014**, *250*, 90–97.

(6) Fujita, S.; Kamazawa, K.; Yamamoto, S.; Tyagi, M.; Araki, T.; Sugiyama, J.; Hasegawa, N.; Kawasumi, M. Proton Conductivity under Dry Conditions for Mesoporous Silica with Highly Dense Sulfonic Acid Groups. *J. Phys. Chem. C* **2013**, *117*, 8727−8736.

(7) Li, G.; Xie, J.; Cai, H.; Qiao, J. New Highly Proton-conducting Membrane Based on Sulfonated Poly(arylene ether sulfone)s Containing Fluorophenyl Pendant Groups, for Low-temperature Polymer Electrolyte Membrane Fuel Cells. *Int. J. Hydrogen Energy* **2014**, *39*, 2639−2648.

(8) Fu, L. C.; Xiao, G.Y.; Yan, D. Y. High Performance Sulfonated Poly(arylene ether phosphine oxide) Membranes by Self-protected Cross-linking for Fuel Cells. *J. Mater. Chem.* **2012**, *22*, 13714–13722.

(9) Peckham, T. J.; Holdcroft, S. Structure-Morphology-Property Relationships of Non-Perfluorinated Proton-Conducting Membranes. *Adv. Mater.* **2010**, *22*, 4667–4690.

(10) Hoarfrost, M. L.; Tyagi, M. S.; Segalman, R. A.; Reimer, J. A. Effect of Confinement on Proton Transport Mechanisms in Block Copolymer/Ionic Liquid Membranes. *Macromolecules* **2012**, *45*, 3112−3120.

(11) Dishari, S. K.; Hickner, M. A. Confinement and Proton Transfer in NAFION Thin Films. *Macromolecules* **2013**, *46*, 413−421.

(12) Kim, O.; Jo, G.; Park, Y. J.; Kim, S.; Park, M. J. Ion Transport Properties of Self-Assembled Polymer Electrolytes: The Role of Confinement and Interface. *J. Phys. Chem. Lett.* **2013**, *4*, 2111−2117.

(13) Paul, D. K.; Fraser, A.; Pearce, J.; Karan, K. Understanding the Ionomer Structure and the Proton Conduction Mechanism in PEFC Catalyst Layer: Adsorbed Nafion on Model Substrate. *ECS Trans*. **2011**, *41*, 1393–1406.

(14) Nagao, Y.; Matsui, J.; Abe, T.; Hiramatsu, H.; Yamamoto, H.; Miyashita, T.; Sata, N.; Yugami, H. Enhancement of Proton Transport in an Oriented Polypeptide Thin Film. *Langmuir*, **2013**, *29*, 6798–6804.

(15) Miyatake, K.; Chikashige, Y.; Higuchi, E.; Watanabe, M. Tuned Polymer Electrolyte Membranes Based on Aromatic Polyethers for Fuel Cell Applications. *J. Am. Chem. Soc.* **2007**, *129*, 3879–3887.

(16) Tan, S.; Belanger, D. Characterization and Transport Properties of Nafion/polyaniline Composite Membranes. *J. Phys. Chem. B* **2005**, *109*, 23480–23490.

(17) Nakamoto, H.; Noda, A.; Hayamizu, K.; Hayashi, S.; Hamaguchi, H.; Watanabe, M. Proton-conducting Properties of a Brønsted Acid-base Ionic Liquid and Ionic Melts Consisting of Bis(trifluoromethanesulfonyl)imide and Benzimidazole for Fuel Cell Electrolytes. *J. Phys. Chem. C* **2007**, *111*, 1541–1548.

(18) Robertson, N. J.; Kostalik, H. A.; Clark, T. J.; Mutolo, P. F.; Abruna, H. D.; Coates, G. W. Tunable High Performance Cross-Linked Alkaline Anion Exchange Membranes for Fuel Cell Applications. *J. Am. Chem. Soc.* **2010**, *132*, 3400–3404.

(19) Krishnan, K.; Iwatsuki, H.; Hara, M.; Nagano, S.; Nagao, Y. Proton Conductivity Enhancement in Oriented, Sulfonated Polyimide Thin Films. *J. Mater. Chem. A* **2014**, *2*, 6895– 6903.

(20) Qiao, J.; Okada, T.; Ono, H. High Molecular Weight PVA-modified PVA/PAMPS Proton-Conducting Membranes with Increased Stability and their Application in DMFCs. *Solid State Ionics* **2009**, *180*, 1318–1323.

(21) Tonozuka, I.; Yoshida, M.; Kaneko, K.; Takeoka, Y.; Rikukawa, M. Considerations of Polymerization Method and Molecular Weight for Proton-conducting Poly(p-phenylene) Derivatives. *Polymer* **2011**, *52*, 6020–6028.

(22) Zhang, J.; Zhou, T.; Qiao, J.; Liu, Y.; Zhang, J. Hydroxyl Anion Conducting Membranes Poly(vinyl alcohol)/poly(diallyldimethylammonium chloride) for Alkaline Fuel Cell Applications: Effect of Molecular Weight. *Electrochimica Acta* **2013**, *111* 351– 358.

(23) Yang, J. S.; Cleemann, L.N.; Steenberg, T.; Terkelsen, C.; Li, Q. F.; Jensen, J. O.; Hjuler, H. A.; Bjerrum, N. J.; He, R. H. High Molecular Weight Polybenzimidazole Membranes for High Temperature PEMFC. *Fuel Cells* **2014**, *14*, 7–15.

(24) Salleo, A.; Kline, R. J.; DeLongchamp, D. M.; Chabinyc, M. L. Microstructural Characterization and Charge Transport in Thin Films of Conjugated Polymers. *Adv. Mater*. **2010**, *22*, 3812–3838.

(25) Sirringhaus, H.; Bird, M.; Zhao, N. Charge Transport Physics of Conjugated Polymer Field-Effect Transistors. *Adv. Mater*. **2010**, *22*, 3893–3898.

(26) Chen, M. S.; Niskala, J. R.; Unruh, D. A.; Chu, C. K.; Lee, O. P.; Frechet, J. M. J. Control of Polymer-Packing Orientation in Thin Films through Synthetic Tailoring of Backbone Coplanarity. *Chem. Mater.* **2013**, *25*, 4088−4096.

(27) Bass, M.; Beman, A.; Singh, A.; Konovalov, O.; Freger, V. Surface Structure of Nafion in Vapor and Liquid. *J. Phys. Chem. B* **2010**, *114*,3784−3790.

(28) Bass, M.; Beman, A.; Singh, A.; Konovalov, O.; Freger, V. Surface-Induced Micelle Orientation in Nafion Films. *Macromolecules* **2011**, *44*, 2893−2899.

(29) Wakita, J.; Sekino, H.; Sakai, K.; Urano, Y.; Ando, S. Molecular Design, Synthesis, and Properties of Highly Fluorescent Polyimides. *J. Phys. Chem. B* **2009**, *113*, 15212–15224.

(30) Hasegawa, T. Advanced Multiple-angle Incidence Resolution Spectrometry for Thin-layer Analysis on a Low-refractive-index Substrate. *Anal. Chem*. **2007**, *79*, 4385–4389.

(31) Hasegawa, T. A Novel Measurement Technique of Pure Out-of-plane Vibrational Modes in Thin Films on a Nonmetallic Material with No Polarizer. *J. Phys. Chem. B* **2002**, *106*, 4112–4115.

(32) Wakita, J.; Jin, S.; Shin, T. J.; Ree, M.; Ando, S. Analysis of Molecular Aggregation Structures of Fully Aromatic and Semialiphatic Polyimide Films with Synchrotron Grazing Incidence Wide-Angle X-ray Scattering. *Macromolecules* **2010**, *43*, 1930–1941.

(33) Miyamae, T.; Tsukagoshi, K.; Matsuoka, O.; Yamamoto, S.; Nozoye, H. Surface Characterization of Polyamic Acid and Polyimide Films Prepared by Vapor Deposition Polymerization by Using Sum-Frequency Generation. *Langmuir* **2001**, *17*, 8125–8130.

(34) Sung, J.; Kim, D.; Whang, C. N.; Oh-e, M.; Yokoyama, H. Sum-Frequency Vibrational Spectroscopic Study of Polyimide Surfaces Made by Spin Coating and Ionized Cluster Beam Deposition. *J. Phys. Chem. B* **2004**, *108*, 10991–10996.

(35) Kakuda, H.; Okada, T.; Hasegawa, T. Anisotropic Molecular Structure in Dip-Coated Films of Linear Poly(ethylene imine) Studied by Infrared Multiple-Angle Incidence Resolution Spectrometry. *J. Phys. Chem. B* **2008**, *112*, 12940–12945.

(36) Matsunaga, M.; Suzuki, T.; Yamamoto, K.; Hasegawa, T. Molecular Structure Analysis in a Dip-Coated Thin Film of Poly(2-perfluorooctylethyl acrylate) by Infrared Multiple-Angle Incidence Resolution Spectrometry. *Macromolecules* **2008**, *41*, 5780–5784.

(37) Hasegawa, T. A New Spectroscopic Tool for Surface Layer Analysis: Multiple-angle Incidence Resolution Spectrometry. *Anal. Bioanal. Chem*. **2007**, *388*, 7–15.

(38) Perez, M. A.; Ren, Y.; Farris, R. J.; Hsu, S. L. Characterization of PMDA-ODA Polyimide Films by External Reflectance Infrared Spectroscopy. *Macromolecules* **1994**, *27*, 6740–6745.

Table of Contents Graphic